Dzyaloshinskii-Moriya interaction probed by magnetization reversal in bilayer Pt/Co/Ir/Co/Pt synthetic ferrimagnets

R. Morgunov, A. Bezverkhnii, Michel Hehn, Jean-Loïs Bello, Thibaud Fache, Stéphane Mangin

Dzyaloshinskii-Moriya interaction probed by magnetization reversal in bilayer Pt/Co/Ir/Co/Pt synthetic ferrimagnets

R. B. Morgunov,[1,2,*] A. I. Bezverkhnii,[1] M. Hehn,[3] J. L. Bello,[3] T. Fache,[3] and S. Mangin[3]
[1]*Institute of Problems of Chemical Physics, 142432 Chernogolovka, Russia*
[2]*I. M. Sechenov First Moscow State Medical University, Ministry of Health of Russia, 119991 Moscow, Russia*
[3]*Institut Jean Lamour, (UMR-CNRS 7198), Université de Lorraine, 54506 Vandœuvre-lès-Nancy, France*

(Received 27 April 2021; revised 6 July 2021; accepted 11 October 2021; published 22 October 2021)

Here, we study the effect of the Dzyaloshinskii-Moriya interaction (DMI) on magnetic nuclei expansion in Pt/Co/Ir/Co/Pt perpendicular synthetic ferrimagnets. Magnetization reversal is explored as a response to the DMI, affecting the expansion of the magnetic nuclei. We report a nontrivial inverted dependence of the velocity of the double domain wall on the in-plane (IP) magnetic field. This effect is due to competition of the DMI contributions, resulting in effective fields of different signs in the two Co layers. We report a macroscopic manifestation of the DMI as magnetization reversal accelerated by the applied IP magnetic field. Accelerated magnetic relaxation is provided by the DMI-induced ellipticity of the magnetic nuclei, the spreading of which is accompanied by an enhanced number of nuclei contacts in comparison with round nuclei in the absence of an IP field. The obtained results clarify how the DMI contributes to macroscopic magnetic relaxation in the presence of the interlayer Heisenberg exchange interaction in synthetic ferrimagnets with perpendicular anisotropy.

DOI: 10.1103/PhysRevB.104.134424

I. INTRODUCTION

The Dzyaloshinskii-Moriya antisymmetric exchange interaction (DMI) attracts scientific attention because of its fundamental origin related directly to the symmetry of matter. For a long time, the DMI—appearing in different types of magnets—has been one of the mysterious problems of magnetism. Artificially separating the generalized exchange interaction into an antisymmetric DMI part **D** and a symmetric Heisenberg part **J** is a common approach to describing interspin coupling controlled by the Pauli principle, and multiple reviews have described the following necessary conditions for DMI existence [1–3]:

(1) There should be a lack of structural inversion symmetry. This requirement sometimes relates to local symmetry. In perovskitelike crystals, where inversion symmetry is present, the DMI exists because of a local lack of this symmetry in the vicinity of the magnetic ions [4].

(2) No DMI can be observed in media in which uncorrelated spins are present.

(3) The exchange interspin coupling should be indirect. This may be either superexchange (as in the original work by Dzyaloshinskii and Moriya) or the Ruderman-Kittel-Kosuya-Yosida (RKKY) interaction [1–3] (as shown by Fert and Levi).

(4) Spin-orbit coupling (SOC) is extremely important [4]. As shown at the outset of research into the DMI, SOC should perturb the localized orbital states of two ions with spins $\mathbf{S}_1$ and $\mathbf{S}_2$. The DMI energy $-\mathbf{D}(\mathbf{S}_1 \times \mathbf{S}_2)$ results in orthogonal mutual spin orientation, while the symmetric Heisenberg part $-\mathbf{J}(\mathbf{S}_1 \times \mathbf{S}_2)$ favors collinear spin alignment. Noncollinear and/or helical magnetism caused by the DMI has been found in spin glasses, manganites, orthoferrites, superconducting cuprates, and noncentrosymmetric single crystals with MnSi crystal structure (see the detailed review in Ref. [3]).

Understanding the origin of the DMI requires controllable variations of the aforementioned factors in experiments. Impressive methods of chemical engineering have been developed for molecular magnets, and controllable regulation of the ligand fields and exchange coupling is now possible because of the variable chemical bonds in metal-organic noncentrosymmetric single crystals manifesting spin chirality [5,6]. Chemical design of metal-organic compounds is a powerful tool for analyzing the DMI.

Another tool for controlling the parameters that determine the intensity of the DMI comes in the form of thin film techniques. It has been shown that the DMI generates skyrmion lattices and other exotic spin textures in thin films [1]. The DMI arises in thin ferromagnetic films at the interface with heavy metals, where SOC [1,3] of two adjacent spins $\mathbf{S}_i$ and $\mathbf{S}_j$ of the ferromagnetic film propagate through the exchange interaction with a heavy metal atom located in an adjacent nonmagnetic layer. This type of DMI implies the absence of inversion symmetry in the interface area and is described in the framework of the three-site Lévy-Fert model [7]. The DMI plays an important role in ferromagnetic and antiferromagnetic spintronics [8,9].

DMI interfaces have been studied experimentally in a wide range of Co-based samples. The asymmetry of bubble expansion in an in-plane (IP) field is a common indicator, allowing estimation of DMI energies D in the range of 0.5–2.5 $\mathrm{mJ/m^2}$ in Pt/Co/Ir/Pt [10], Pt/Co/Ir [11,12], and Pt/Co/Pt [13,14]. The values depend on the Co layer thickness, the interface quality textures, and the type of spacer. Normally, dependence of the

*morgunov2005@yandex.ru

velocity of the double domain wall (DDW) on the IP magnetic field $v(\mu_0 H_{IP})$ has a negative curvature and a shape close to that of a parabola. In all the single-layer Co systems, the minima of the $v(\mu_0 H_{IP})$ dependences shift from zero under an IP field because of the DMI contribution to the domain-wall (DW) dynamics. Another system known to allow estimation of the DMI at room temperature is a Co superlattice manifesting skyrmions [15–17]. The DMI coupling energy has been analyzed by magnetic force microscopy in $[Pt/Co/Pt]_{13}$ [16], $[Ir/Co/Pt]_{10}$ [15], and $Pt/[Ir/Co/Pt]_5/Pt$ [17] superlattices. In the aforementioned publications, either exchange-isolated Co layers [10–14] or exchange-coupled layers [15–17] are analyzed, but the literature is lacking studies of the DMI effect on magnetic nuclei expansion in exchange-coupled double ferromagnetic layers.

In multilayers comprising two ferromagnetic layers separated by a nonmagnetic conducting spacer, there can be indirect exchange interaction between the two ferromagnetic layers, the origin of which is the RKKY interaction. The sign of the interlayer exchange interaction alternates with the spacer thickness, resulting in either a parallel or antiparallel exchange coupling constant. A double-layer sample combining the interlayer Heisenberg interaction and the interfacial DMI is a complicated and sophisticated system because the relationship between the symmetric and antisymmetric parts of the exchange interaction remains unclear, as does the participation of the free electrons in providing the DMI [18]. Special attention is focused on analyzing how the interlayer spacer and ferromagnetic layer thicknesses affect the DMI and Heisenberg strengths [19]. These parameters affect the fine microscopic details of the dynamics and spin relaxation of the RKKY electrons, transferring spin polarization.

In this paper, Pt/Co (1.1 nm)/Ir (1.4 nm)/Co (t_{Co})/Pt structures, with $t_{Co} = 0.6$, 0.7, 0.8, and 1.0 nm, are analyzed because their single-layer analogues are well known for providing the DMI effect on bubble expansion. The thickness of the Ir spacer is chosen so that antiferromagnetic coupling occurs between the two Co layers. Consequently, four equilibrium magnetic states are stabilized depending on the magnetic field history (see Fig. S1 in the Supplemental Material [20]): two states with parallel orientation of the layer magnetizations P^+ ($\uparrow\uparrow$) and P^- ($\downarrow\downarrow$) and two with antiparallel orientation AP^+ ($\downarrow\uparrow$) and AP^- ($\uparrow\downarrow$), which are not equivalent because of the different Co layer thicknesses. In ($\uparrow\uparrow$), ($\downarrow\downarrow$), ($\downarrow\uparrow$), and ($\uparrow\downarrow$), the first arrow corresponds to the thin-layer magnetization, while the second corresponds to the thick-layer magnetization (close to the substrate). Due to using different thicknesses for the two Co layers, the four levels in the Kerr loops or Kerr images allow the magnetic state to be identified (see Fig. S1 in the Supplemental Material [20]). Interstate transitions occur through nucleation and propagation of DWs, and the transitions among the P^+, P^-, AP^+, and AP^- states depend on interdomain interactions controlled by the surrounding phases and their contacts with each other [21]. We refer to the border containing two DWs in two layers as a DDW to distinguish it from the single DW in a monolayer sample.

Nonmonotonic magnetic relaxation [22] and movement of DWs opposite to the Zeeman force direction [21] illustrate the complexity of coupled DWs and their unusual dynamics. Surprisingly, increasing the out-of-plane (OP) applied field can decrease and even change the sign of the DDW velocity [23].

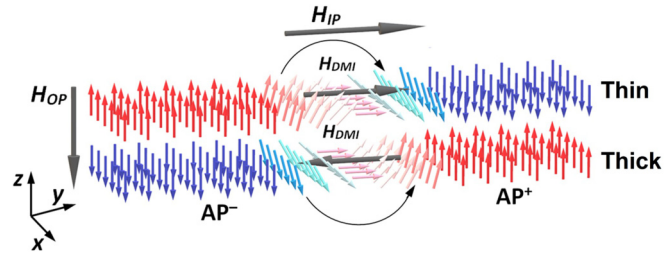

FIG. 1. Sketch of spin structures near the double domain wall (DDW) of AP^-/AP^+ type in the thin and thick layers of a synthetic ferrimagnet. The directions of spin rotation are shown by the circling arrows. The thin and thick ferromagnetic layers are coupled by a negative Ruderman-Kittel-Kosuya-Yosida interaction.

During the $AP^+(\downarrow\uparrow) \rightarrow AP^-(\uparrow\downarrow)$ transition, DWs in the upper Co layer separate areas with magnetization of $\uparrow$ type from the environment with magnetization of $\downarrow$ type, while in the thick Co layer, DWs separate areas of $\downarrow$ type surrounded by areas with $\uparrow$ type of magnetization (Fig. 1). As shown in Fig. 1, applying a magnetic field in the $-z$ direction increases the energy of the thin layer while decreasing that of the thick layer.

Although the DWs in the thick and thin layers move simultaneously in the same direction, this direction is controlled mainly by the thicker layer because of its higher Zeeman energy. The DW in the thick layer is under an extensive force, whereas that in the thin layer is under a compressive force.

When the interfacial or interlayer DMI is present, different directions of spin rotation within DWs should be considered. Because the symmetries of the DMI and the Heisenberg exchange interaction J are different [24], opposite directions of spin rotation in the thin and thick layers (Fig. 1) change the sign of the DMI energy density D, while the symmetric part of the exchange interaction J remains constant [24]. Herein, we show that the difference in signs of the DMI in the thin and thick Co layers leads to nonmonotonic variation of the total energy of the DDW in an external field and causes a nontrivial field dependence of the velocity of the DDW of AP^-/AP^+ type when the field is applied in the film plane.

The aim of this paper is to reveal the DMI contributions to magnetization reversal analyzed by the dynamics of integral magnetization and individual DDWs in a ferrimagnetic synthetic structure comprising two exchange-coupled ferromagnetic Co layers of different thicknesses in contact with Ir and Pt heavy metals.

II. EXPERIMENTAL TECHNIQUE

A. Samples

Measurements were made on Si/SiO_2 (100 nm)/Pt (3.2 nm)/Co (1.1 nm)/Ir (1.4 nm)/Co (t_{Co})/Pt (3.2 nm) synthetic ferrimagnets with perpendicular magnetic anisotropy (PMA) in multilayers. While the thickness of the thick Co layer was fixed to 1.1 nm, that of the thin Co layer (t_{Co}) was varied among 0.6, 0.7, 0.8, and 1.0

nm. The PMA originates from the hybridization of the 3*d* orbital moment of Co and the 5*d* ones of Pt and Ir [25]. The relatively thin Co layers (∼1 nm) provide the dominance of surface magnetic anisotropy over bulk anisotropy and enhance the effect of the DMI. The high quality of the interfaces was confirmed by small-angle x-ray diffraction (see Fig. S2 in the Supplemental Material [21]). The Ir thickness was fixed at $t_{Ir} = 1.4$ nm, corresponding to the second peak of RKKY antiferromagnetic coupling vs t_{Ir}. The thickness of the Ir spacer was tuned so that the Heisenberg interlayer exchange interaction was strong enough to provide the DDW structure without it separating into two single DWs belonging to each Co layer. The energy balance prevented DW separation: the Zeeman energy stimulating DW motion ($E_Z \sim 1.3 \times 10^{-2}$ mJ/m^2 in magnetic field $\mu_0 H_{OP} \sim$ –60 mT) was lower than the interlayer exchange coupling $E_{EX} \sim 0.1$ mJ/m^2, which is why, in our experiments, there were no external fields strong enough to separate the DDW into independent DWs. Herein, we discuss DDW movement only.

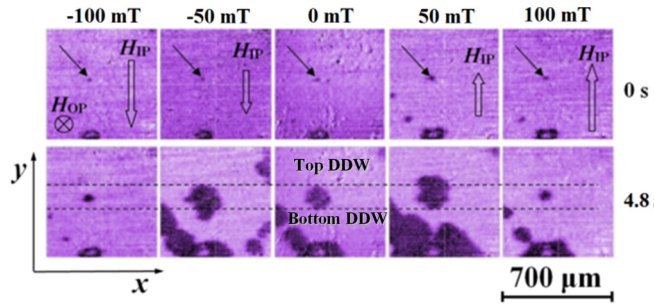

FIG. 2. Magneto-optic Kerr effect (MOKE) images of sample with $t_{Co} = 1$ nm at constant out-of-plane (OP) field $\mu_0 H_{OP} = -57.8$ mT and varying in-plane (IP) field H_{IP}. The top line contains images of the initial state at $t = 0$, when $\mu_0 H_{OP}$ was switched to −57.8 mT and $\mu_0 H_{IP}$ was switched to −100, −50, 0, 50, or 100 mT; the initial nucleated domain positions are marked by arrows. The bottom line contains images recorded after 4.8 s. The brighter areas correspond to the AP$^+$ state, while the darker areas correspond to the AP$^-$ state. The horizontal dashed lines allow comparison of the displacements of the top and bottom double domain wall (DDW) in different fields.

B. Magnetic bubble expansion technique

Measurements of the DW velocity [10,11,13] were performed using a Durham Magneto-optics NanoMOKE3 microscope based on the magneto-optical polar Kerr effect (MOKE). A quadrupole electromagnet allowed us to set the IP and OP field components independently, and expansion of the magnetic nuclei was studied in a constant magnetic field without short impulses. Measurements were performed for a field range in which the resulting balance of Zeeman and exchange energies favored expansion of the AP$^-$ phase. The procedure for all samples was the same as that described here for the sample with $t_{Co} = 1$ nm, but of course the actual values of the operating fields depended on the value of t_{Co}. First, the sample was brought into the P$^+$ state with an OP magnetic field of $\mu_0 H_{OP} = +80$ mT. Then the applied field was changed to be close to that allowing the AP$^+ \rightarrow$ AP$^-$ transition. In Fig. 2, $\mu_0 H_{OP}$ is equal to −57.8 mT (see Fig. S1(d) in the Supplemental Material [20]). Simultaneously, a constant field H_{IP} was applied in the plane of the sample along the *y* axis (IP field). As shown in Fig. 2 for the sample with $t_{Co} = 1$ nm, the domain structure was recorded by a Kerr microscope at intervals of 0.6 s. This sequence was repeated with values of $\mu_0 H_{IP}$ from −100 to +100 mT at intervals of 5 mT. The position of the DDW was determined in each image, and we simultaneously observed three types of nuclei distinguished by their brightness and whose shapes were close to circular in the MOKE images.

The velocities of the DDW were determined from the slopes of its position *y* as a function of time [see $y(t)$ dependences in Fig. 3]. Multiple examples of the $y(t)$ dependences for different fields are shown in Fig. S3 of the Supplemental Material [20]. The error of ±6.6 μm in the $y(t)$ dependences was determined from analyzing five independent nuclei, the expansions of which were observed under the same conditions. In Figs. 2 and 3, the difference between the top and bottom DDW velocities can be seen in the presence of the IP field.

Each experimental $y(t)$ dependence provides values for the bottom and top DDW velocities. Thus, we determined the AP$^-$/AP$^+$ DDW velocities from the slopes of the $y(t)$ dependences, accurately verifying their linearity in each experiment.

C. Dynamics of magnetization reversal

The dynamics of magnetization reversal, i.e., the time dependences of the magnetic moment, were recorded using an MPMS XL Quantum Design SQUID magnetometer. First, the sample magnetization was saturated in a field of $\mu_0 H_{OP} =$ 400 mT, exceeding the saturation field that varied in the range of 65–140 mT for the different samples. This provided the P$^+$ unified initial state in all the analyzed samples. After saturation, we switched the permanent OP field $\mu_0 H_{OP}$ to

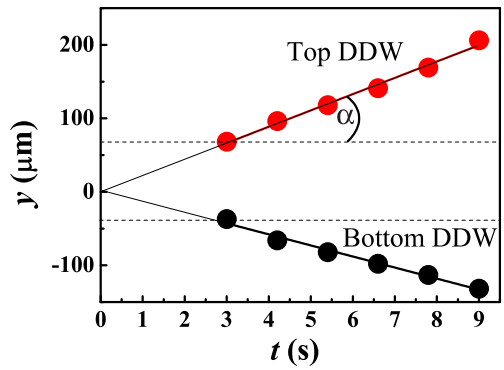

FIG. 3. Typical time dependences of the *y* coordinate of the double domain wall (DDW) between AP$^-$ and AP$^+$ phases with an out-of-plane (OP) field of $\mu_0 H_{OP} = -57.8$ mT and an in-plane (IP) field of $\mu_0 H_{IP} = -20$ mT for the sample with $t_{Co} = 1.0$ nm (see Fig. 2). The initial coordinates of the domain walls (DWs) at $t = 0$ are shown by the horizontal dashed lines. The coordinate $y = 0$ corresponds to the nucleation point shown by the arrow in Fig. 2. The size of the experimental points corresponds to that of the errors.

the opposite direction. The absolute value of the decreased field was close to the switching field, corresponding to the $AP^+ \rightarrow AP^-$ transition. We determined this value in advance from the magnetic hysteresis recorded for each sample. Stabilization of the $\mu_0 H_{OP}$ field took 60 s, which was much shorter than the subsequent relaxation time of ~40 min. After field stabilization, we acquired data on the time variation of the net magnetization of the whole sample. Thus, the relaxation dynamics were measured in the static field regime.

The H_{IP} and H_{OP} components of the field depended on each other in this series of experiments. The sample was installed in the SQUID magnetometer at the desired angle θ between the sample perpendicular and the magnetometer field. This orientation gives the ratio of the IP and OP components as $H_{IP}/H_{OP} = \tan\theta$. Because we studied the effect of the IP field on magnetic reversal, the OP component had to be constant. For that purpose, when analyzing the effect of the IP component on magnetic relaxation, the intensity of the field was changed such that the OP component H_{OP} was always constant. In the other series of experiments, in which the effect of the OP component on magnetization reversal was studied, the IP field was absent, and the OP component was varied to change the mode of magnetic relaxation.

III. RESULTS AND DISCUSSION

A. Asymmetric expansion of AP^+/AP^- border under IP field

The driving force of DW movement in ultrathin films with PMA is the magnetic field directed along the easy axis, i.e., the field H_{OP} perpendicular to the film. The IP field changes the energy of the DWs, but in the absence of the DMI, the IP field does not provide asymmetry of magnetic nuclei expansion [13].

In the presence of the DMI, the effective field comprises the constant external field H_{IP} and the directed IP field H_{DMI} of the sample. The effective IP field of the sample affects the velocities of the DWs, and this fact can be used to estimate the strength and sign of the DMI [10,13]. The equation for DW motion in creep mode is used to find the relationship between the DW velocity v and the field H_{DMI}, i.e.,

$$v = v_0 \exp[-\zeta(\mu_0 H_{OP})^{-1/4}], \quad (1)$$

where v_0 is the constant velocity, and ζ is a scaling coefficient. According to Ref. [13], ζ depends on the energy density σ of the DW controlled by the IP field H_{IP}, i.e.,

$$\zeta = \zeta_0[\sigma(H_{IP})/\sigma_0]^{1/4}, \quad (2)$$

where ζ_0 is a scaling coefficient, σ is the DW energy density [13], and σ_0 is the energy density of a Bloch-type DW. Equation (2) is a measure of the deviation of the DW energy from that of a Bloch-type DW. Applying the IP field induces a gradual transformation of a Bloch DW to a Néel DW, and generally, the DW is encountered in a state between the Bloch and Néel spin configurations. The energy density $\sigma(H_{IP})$ of the intermediate DW configuration decreases with the IP field, and σ depends on the DMI energy accordingly as [13]

$$\sigma(H_{IP}) = \sigma_0 - \frac{\pi^2 \Delta \mu_0 M_S^2}{8K_D}(H_{IP} + H_{DMI})^2. \quad (3)$$

Equation (3) is valid if the sum of the external field H_{IP} and the effective DMI field H_{DMI} is small enough for the DW to be described by the Bloch model, i.e., $|H_{IP} + H_{DMI}| < 4K_D/\pi\mu_0 M_S$, where $\Delta = (A/K)^{1/2} = 6.86$ nm is the DW width, $K_D = N_x \mu_0 M_S^2/2 = 2.7 \times 10^4$ mJ/m^2 is the anisotropy energy density in the analyzed sample with $t_{Co} = 1.0$ nm nm, and $N_x = \ln(2)t_{Co}/(\pi\Delta)$ is the demagnetizing factor of the DW. If the DMI is strong such that $|H_{IP} + H_{DMI}| > 4K_D/\pi\mu_0 M_S$, then the DW is closer to the Néel type, and the energy density in a Néel wall is given by

$$\sigma(H_{IP}) = \sigma_0 - 2\Delta K_D - \pi\Delta\mu_0 M_S|H_{IP} + H_{DMI}|. \quad (4)$$

Substituting Eq. (3) or Eq. (4) into Eq. (2) and then Eq. (2) into Eq. (1) describes the dependence of the single-DW velocity on the IP field H_{IP}. The dependence $v(\mu_0 H_{IP})$ has a minimum at $H_{IP} = -H_{DMI}$, i.e., compensating the effective DMI field by the external IP field results in the minimum DW velocity, so the DW velocity can be used to measure the intrinsic DMI field. In a single Co layer, the minimum of the $v(\mu_0 H_{IP})$ dependence occurs when the IP field equals the DMI effective field [10–14], but it is difficult to say *a priori* how the DMI affects the $v(\mu_0 H_{IP})$ dependence in bilayer samples.

In the Co bilayer with $t_{Co} = 1.0$ nm, typical experimental dependences of the velocity projection on the y axis $v_y(\mu_0 H_{IP})$ for the DDW of the AP^+/AP^- type were measured for the top and bottom DDWs belonging to the same nucleus [Fig. 4(a)]. In Fig. 4, the errors were determined as 0.2–0.9 μm/s from analyzing five or six independent measurements and are smaller than the experimental points.

The bottom DDW, moving against the IP field, demonstrates the asymmetric $v_y(\mu_0 H_{IP})$ dependence with a maximum at $\mu_0 H_{IP} = -30$ mT, while the maximum of the $v_y(\mu_0 H_{IP})$ dependence of the top DDW, moving along the IP field, is centered at $\mu_0 H_{IP} = 45$ mT. In the samples with $t_{Co} =$ 0.6 and 0.8 nm (see Fig. S4 in the Supplemental Material [20]), the maxima of the $v_y(\mu_0 H_{IP})$ dependences lie outside the available field range (from −100 to +100 mT).

The left and right DDWs of the nucleus have the same transverse velocity v_x. The $v_x(\mu_0 H_{IP})$ dependence is symmetric and centered at $H_{IP} = 0$. The left and right parts of the $v_x(\mu_0 H_{IP})$ dependence are close to a linear function corresponding to the creep mode [Fig. 4(b)]. The experimental dependences $v(\mu_0 H_{IP})$ in a bilayer sample are found to be quite different from those described in the literature for single-layer samples [10–14].

We analyzed the field dependences of the DDW velocities in the frame of formalism developed in Ref. [13]. We assume a DDW comprising two DWs belonging to the thick and thin Co layers (Fig. 1). Magnetization reversal corresponding to the $AP^+ \rightarrow AP^-$ transition is produced by simultaneous movement of the two DWs in the same direction because they are coupled by interlayer RKKY exchange. The spin rotations in these two DWs are opposite to each other (Fig. 1). For that reason, the effective field $H_{IP} + H_{DMI}$ directed along the y axis increases the energy of the DW in the thick layer and decreases that of the DW in the thin layer. One can say that the effective field pulls the DWs belonging to the same DDW in opposite directions. Thus, the total energy density σ of the DDW can be expressed by summing the corresponding

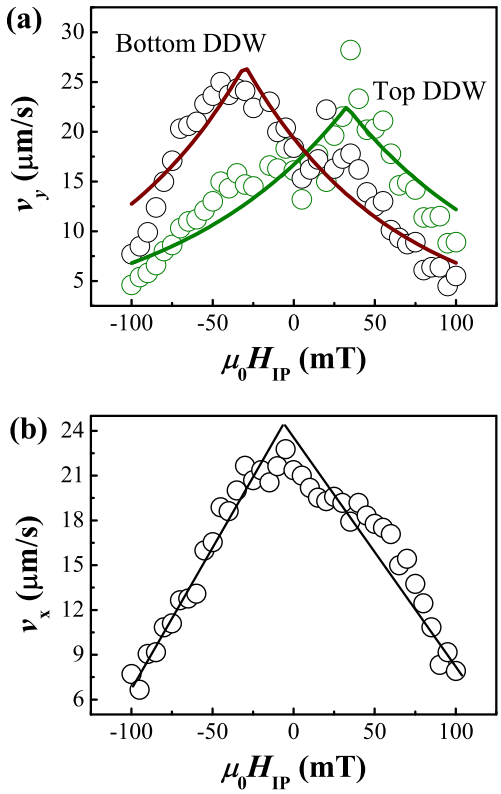

FIG. 4. (a) Projections of velocity v_y of top and bottom double domain wall (DDW) and (b) transverse projection of velocity v_x of the DDW as functions of the in-plane (IP) field H_{IP} applied along the y axis (see Fig. 2). The size of the experimental points corresponds to the error. Experiments (a) and (b) were carried out with the $t_{Co} = 1$ nm sample in the presence of a constant out-of-plane (OP) field of $\mu_0 H_{OP} = -57.8$ mT. The solid lines are the approximations described in the text.

contributions from the two layers, i.e.,

$$\sigma(H_{IP}) = \sigma_0 - 2\Delta_1 K_{D1} - \pi\Delta\mu_0 M_{S1}|H_{IP} + H_{DMI1}| - 2\Delta_2 K_{D2} - \pi\Delta\mu_0 M_{S2}|H_{IP} - H_{DMI2}|, \quad (5)$$

where indices 1 and 2 correspond to the single DWs in the thin and thick layers, respectively.

The approximations shown by the solid lines in Fig. 4(a) allow one to extract $\mu_0|H_{DMI}| = 85.2$ mT in the thick layer and $\mu_0|H_{DMI}| = 99.5$ mT in the thin layer. The corresponding values of the DMI energy density $D = \Delta\mu_0 M_S H_{DMI}$ are $D_{thick} = 0.76\,\mathrm{mJ/m^2}$ and $D_{thin} = 0.88\,\mathrm{mJ/m^2}$. These parameters confirm validity of the expression $|H_{IP} + H_{DMI}| > 4K_D/\pi\mu_0 M_S (4K_D/\pi\mu_0 M_S = 10.8\,\mathrm{mT})$, corresponding to the DW of the Néel type. Considering the opposite spin rotations in the top and bottom DDWs within the standard model developed for a single Néel DW allows one to describe the experimental dependences in a bilayer structure, assuming the contributions of each layer [Fig. 4(a)].

B. Effect of IP magnetic field on magnetization reversal

We studied the dynamics of the magnetization reversal in a constant magnetic field as described in Refs. [21,22] and in Sec. II. Nonmonotonic magnetic relaxation in a series of Pt/Co/Ir/Co/Pt samples analyzed in this paper was reported and discussed in Refs. [21,22]. The dynamic system of differential equations in Eq. (6) proposed in Ref. [21] describes oscillations of a macroscopic net of magnetic moment. The three phases P^-, AP^-, and AP^+ can coexist simultaneously, with corresponding proportions $\widetilde{P^-}$, $\widetilde{AP^-}$, and $\widetilde{AP^+}$. The proportions $\widetilde{P^-}$ and $\widetilde{AP^-}$ arise from conversion of the AP^+ state to either the AP^- or P^- state with probability $\alpha\widetilde{AP^+}$ or $\gamma\widetilde{AP^+}$, respectively. The P^- nuclei can be transferred to AP^- ones with probability $\beta\widetilde{P^-}$. The key point of the model is the nonlinear term $\delta\widetilde{P^-}\widetilde{AP^-}$, which describes the interaction between magnetic nuclei of the P^- and AP^- states. In contrast to other terms that describe the individual behavior of nuclei, the nonlinear term $\delta\widetilde{P^-}\widetilde{AP^-}$ describes the interaction of the P^- nuclei with the AP^- nuclei. The P^- nuclei are incommensurate with the applied field. The P^- phase should not be present in quasistatic slow relaxation between the AP^+ and AP^- phases, but it appears because of its low activation energy even in a field not corresponding to transition in the P^- phase [22]. For that reason, the P^- phase inclined in between the normal AP^- and AP^+ phases affects their dynamics when P^- and AP^- nuclei meet each other. The simultaneous presence of P^- and AP^- nuclei in magnetically relaxing synthetic ferrimagnets causes competition of relaxation channels and interaction among them.

$$\frac{d\widetilde{P^-}}{dt} = \alpha\widetilde{AP^+} - \beta\widetilde{P^-} - \delta\widetilde{P^-}\widetilde{AP^-}$$
$$\frac{d\widetilde{AP^-}}{dt} = \gamma\widetilde{AP^+} + \beta\widetilde{P^-} + \widetilde{P^-}\widetilde{AP^-}$$
$$\widetilde{AP^+} + \widetilde{P^-} + \widetilde{AP^-} = 1. \quad (6)$$

The coefficient α is the frequency of conversion of the initial AP^+ phase to P^- nuclei, β is the frequency of conversion of P^- to AP^-, γ is the frequency of conversion of the initial AP^+ phase to the AP^- nuclei from the initial AP^+ phase, and δ is the frequency of contacts of the expanding AP^- and P^- nuclei.

Because the DMI controls the movement of the DWs as shown in the experiments described above, one can suppose the effect of the DMI on δ in Eq. (6). Because internuclei interaction depends on the nuclei border, δ is an important characteristic of the nuclei interaction, and this parameter can depend on the DMI. Two additional factors become important in a bilayer sample in comparison with earlier considered single-layer films: (i) the number and frequency of contacts of the three magnetic phases, which are present simultaneously in a sample during relaxation and (ii) the DMI appearing in the interphase borders and controlling their expansion and conversion from one to another. We performed a simple test experiment to verify the effect of the DMI on magnetic nuclei interaction and parameter δ corresponding to phase interaction [see Eq. (6)]. Relaxation of the total magnetic moment of the sample with $t_{Co} = 0.7$ nm (Fig. 5) was measured by a SQUID magnetometer in the same manner as in Refs. [21,22], but the external field was directed not perpendicular to the films at $\theta \neq 0°$ (see the inset in Fig. 6). Two projections of the external field were used: the first one $\mu_0 H_{OP} = \mu_0 H\cos\theta$ was a perpendicular projection (OP), and the second one

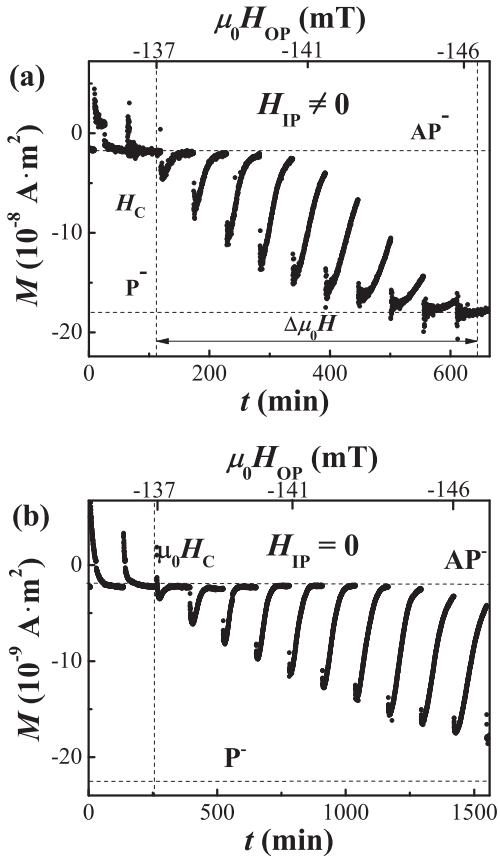

FIG. 5. Series of relaxation curves recorded with similar constant out-of-plane (OP) fields for each pair of relaxation curves presented in (a) and (b) but with different in-plane (IP) fields (a) $\mu_0 H_{IP} = \mu_0 H_{OP} \tan\theta$ and (b) $\mu_0 H_{IP} = 0$ in the sample with $t_{Co} = 0.7$ nm at $T = 100$ K. The upper horizontal line marks the equilibrium magnetic moment in the AP$^-$ state. The vertical dashed line indicates the border of the field range ΔH at which nonmonotonic relaxation is observed.

$\mu_0 H_{IP} = \mu_0 H \sin\theta$ was an IP component. As shown above, a nonzero IP field results in asymmetric DDW movement. In this section, we check whether internuclei interaction expressed by parameter δ in the nonlinear term $\delta\widetilde{P^-}\widetilde{AP^-}$ is sensitive to the DMI and to the IP field.

A series of relaxation curves recorded at $T = 100$ K and $\theta = 33^\circ$ is shown in Fig. 5(a). The range $\Delta\mu_0 H_{OP}$ of the OP field used to plot Fig. 5(a) was the same as that used in Fig. 5(b), although the lengths of the magnetic field vectors shown on the horizontal axis are different. Thus, the difference between the relaxation curves [Figs. 5(a) and 5(b)] is the presence or absence of the IP field, while the OP field is the same for all the relaxation curves. One can find the following features of the relaxation curves: (i) the critical OP field at which nonmonotonic relaxation begins and the range of the OP field corresponding to the nonmonotonic mode are the same independent of the presence of the IP field, i.e., the IP field does not change the key parameters of magnetization reversal, controlled by the Heisenberg interlayer exchange interaction and magnetic anisotropy; and (ii) the shape and duration of the individual relaxation curves are different in the presence and absence of the IP field.

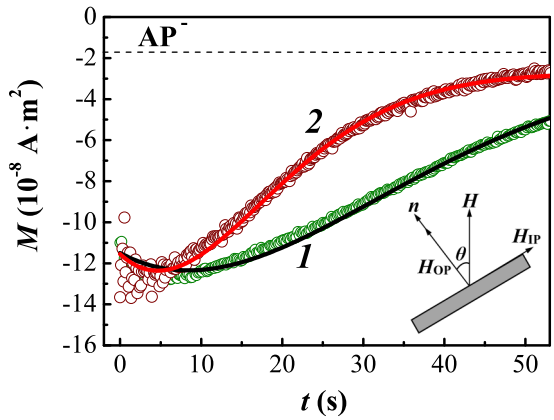

FIG. 6. Time dependences of magnetic moment M from equilibrium asymptotic moment in the AP$^-$ state in the sample with $t_{Co} = 0.7$ nm at $T = 100$ K. The relaxation curves were recorded with the same out-of-plane (OP) field $\mu_0 H_{OP} = -142$ mT but different in-plane (IP) fields $\mu_0 H_{IP} = 0$ (curve 1) and $\mu_0 H_{IP} = -89$ mT (curve 2). The dashed horizontal line indicates the magnetic moment of the final AP$^-$ state. The solid lines are approximations by the solutions of the system in Eq. (6) for $\delta = 4.38 \times 10^{-2}$ (line 1) and $\delta = 5.86 \times 10^{-2}$ (line 2). The sample installation is shown schematically in the inset.

An example of a selected pair of relaxation curves recorded with the same OP magnetic field $\mu_0 H_{OP} = -142$ mT and different IP fields $\mu_0 H_{IP} = 0$ (curve 1) and -89 mT (curve 2) is shown in Fig. 6 for the sample with $t_{Co} = 0.7$ nm at $T = 100$ K. One can conclude that the presence of the IP field accelerates magnetic relaxation, although it is generally assumed in the literature that the driving force of domain expansion is the OP field only. Similar regularities were observed in other samples of the series with $t_{Co} = 0.6$, 0.8, and 1.0 nm at corresponding temperatures satisfying the theoretical conditions for nonmonotonic relaxation [22] (see Figs. S5–S7 in the Supplemental Material [21]). The relaxation curves are approximated by solutions of the dynamic system in Eq. (6) (the solid lines in Figs. 6 and S5–S7).

The approximation shows that the only reason for the relaxation curve changing under the IP field is the increase in δ, corresponding to the frequency of contacts of the simultaneously expanding AP$^-$ and P$^-$ nuclei. Although the IP field does not change the nucleation barrier, the IP field produces the macroscopic effect of accelerating the magnetic relaxation by a factor of as much as $\sim$1.34 because of changes in the parameter δ.

The increase in the frequency of contacts of the simultaneously expanding AP$^-$ and P$^-$ nuclei can be explained by changes in nuclei topology caused by the IP field in the presence of the DMI. As shown in Sec. II B, round domains expand asymmetrically in the presence of the IP field. The parameter $\lambda = a/b$ of domain ellipticity has been introduced [see the inset in Fig. 7(a)], and this parameter is plotted as a function of the IP field [Fig. 7(a)]. Examples of the nuclei shapes in IP fields of 0 and -70 mT are shown in Figs. 7(b) and 7(c), respectively. The asymmetry is calculated with the parameter $a = t(v_{top} + v_{bottom})$, corresponding to the sum of the distances traveled by the top and bottom

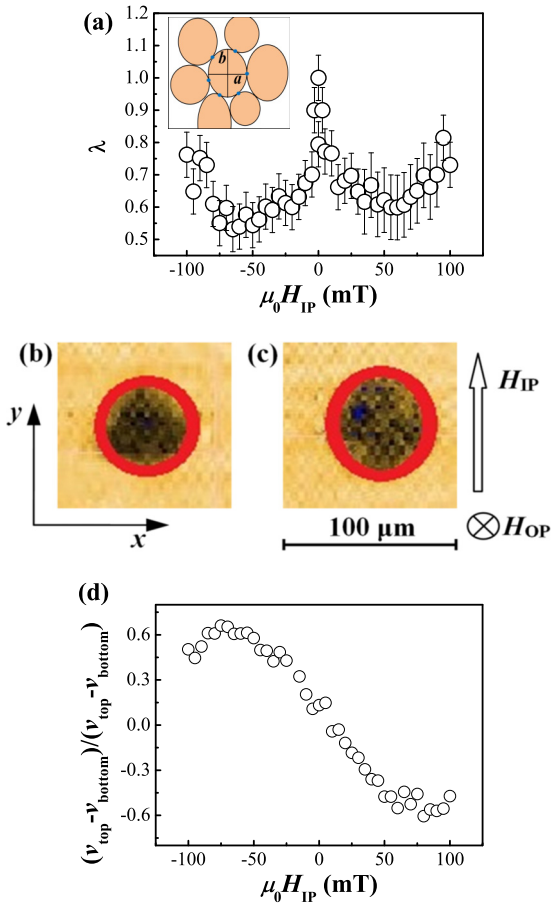

FIG. 7. (a) Dependence of ellipticity $\lambda = a/b$ of magnetic nuclei on the in-plane (IP) magnetic field $\mu_0 H_{IP}$ in the presence of the constant out-of-plane (OP) magnetic field $\mu_0 H_{OP} = -57.8$ mT corresponding to the AP^- state in the sample with $t_{Co} = 1.0$ nm; magneto-optic Kerr effect (MOKE) images of magnetic nucleus in fields (b) $\mu_0 H_{IP} = 0$ mT and (c) $\mu_0 H_{IP} = -70$ mT. The sketch demonstrates the contacts of elliptic nuclei. (d) Dependence of asymmetry $(v_{top} - v_{bottom})/(v_{top} + v_{bottom})$ on the IP magnetic field $\mu_0 H_{IP}$ in the presence of the constant OP magnetic field $\mu_0 H_{OP} = -57.8$ mT, corresponding to the AP^- state in the sample with $t_{Co} = 1.0$ nm. The size of the experimental points corresponds to the error.

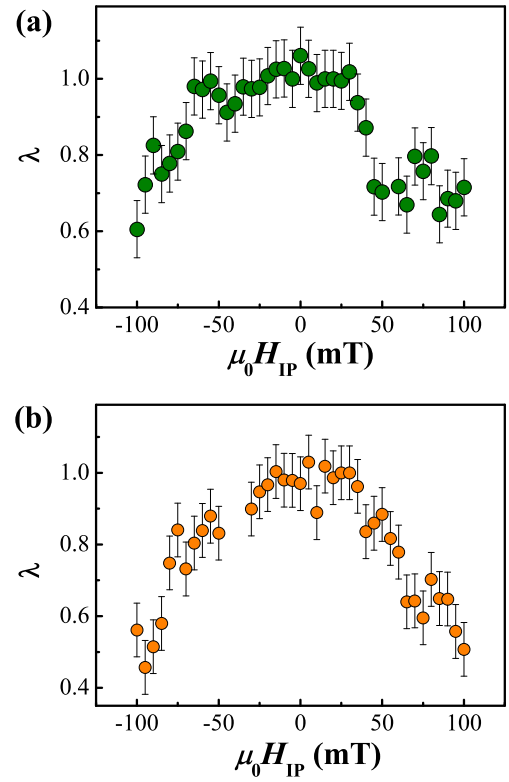

FIG. 8. Dependences of ellipticity λ of the bubble domain on the $\mu_0 H_{IP}$ field in samples with (a) $t_{Co} = 0.6$ nm and (b) $t_{Co} = 0.8$ nm at 300 K.

DDWs along the y axis, where v_{top} is the velocity of the top DDW [see Fig. 4(a)], v_{bottom} is that of the bottom DDW [see Fig. 4(a)], and $b = t v_x$ is the distance traveled by a side DDW along the x axis with velocity v_x [see Fig. 4(b)]. This definition of ellipticity does not coincide with the standard physical definition of nucleus asymmetry characterizing the DMI equal to $(v_{top} - v_{bottom})/(v_{top} + v_{bottom})$ [see Fig. 7(d)]. The $(v_{top} - v_{bottom})t$ difference is mainly used in the literature. This choice provides the possibility of comparing our results with topological ellipticity. This possibility is considered to explain surface covering by ellipses [26]. Figure 7(a) is plotted by averaging four $\lambda(\mu_0 H_{IP})$ curves plotted for each independent nucleus.

The ellipticity decreases from 0.8 (close to round shape) to 0.5 (distorted shape) as the IP field is increased from 0 to 50–60 mT. The subsequent increase in the IP field up to 100 mT causes partial restoration of ellipticity to a value of 0.7–0.8. The ellipticity was determined by averaging five or six values measured in independent experiments, and the corresponding error bars are shown in Fig. 7(a).

Similar $\lambda(\mu_0 H_{IP})$ dependences are found for all samples of the series with different t_{Co} values (see Fig. 8). No minima of the $\lambda(\mu_0 H_{IP})$ dependences are observed in the samples with $t_{Co} = 0.6$ nm [Fig. 8(a)] and $t_{Co} = 0.8$ nm [Fig. 8(b)] because the increase in the IP field up to 100 mT is insufficient to reach the maximum of the $v(t)$ dependence at 300 K. The effective DMI field in these samples exceeds 100 mT. Changes in ellipticity affect the covered area and number of contacting points among neighboring ellipses [26]. The variation in λ from 1.0 at $\mu_0 H_{IP} = 0$ to 0.5 at $\mu_0 H_{IP} = 50$ mT corresponds to a variation in the number of contact points from 4.0 ± 0.1 to $\sim 5.7 \pm 0.2$, as shown by computer modeling using the Monte Carlo technique in Ref. [26].

Magnetic relaxation is accompanied by changes in the average number of closest neighbors. The increase in the IP magnetic field changes the average number of contacts and the corresponding parameter of the nuclei meeting frequency δ by 20–40%. Thus, the DMI affects the ellipticity of nuclei and the frequency of their meeting as well as the covered area of the sample in the presence of the IP field. In the literature, the effect of the DMI on macroscopic integrated magnetic characteristics is comparatively rare. A macroscopic response to the DMI was confirmed indirectly by magnetization reversal measurements in the framework of first-order reversal curve experiments in Pt/Co/MgO and Ir/Fe/Co/Pt multilayers

[27]. Herein, we report on magnetization reversal dynamics affected by the DMI.

IV. CONCLUSIONS

(1) We have revealed the nonmonotonic dependence of the velocity v of the complex DDW in bilayer Pt/Co/Ir/Co/Pt samples on the IP magnetic field. This dependence is inverted in comparison with those observed in single-layer Pt/Co/Ir and Pt/Co/Pt structures. This phenomenon can be explained by competition of the DMI fields controlling the expansion of nuclei in the thick and thin Co layers. The opposite signs of the DMI fields in the thick and thin layers are due to the opposite directions of spin rotation in the corresponding DWs. This causes a maximum of the $v_y(\mu_0 H_{IP})$ dependence, approximation of which results in DMI energy $D = 0.88 \pm 0.23\,\mathrm{mJ/m^2}$ close to the DMI in single-layer Pt/Co/Ir and Pt/Co/Pt structures revealed by other authors.

(2) We have found a macroscopic response of magnetization reversal to the DMI and IP effective magnetic fields. The IP magnetic field, generating asymmetry of magnetic nuclei, in the presence of the DMI increases the number of nuclei average neighbors and the frequency of nuclei contacts by 30–40%. This accelerates the magnetic relaxation of the integrated total magnetic moment of the sample. This phenomenon has been found in all series of the studied samples with varied thickness of the upper Co layer. One can expect generalization of this phenomenon to other synthetic ferrimagnets with the DMI.

(3) Unusual dynamics of the two-stack complex border, separating different magnetic phases in bilayer Co structures, manifest the valuable difference in regularities of simple DW dynamics studied in single-layer synthetic antiferromagnets. We have proposed approaches allowing us to explain features of the interphase border dynamics and DMI manifestation in bilayer samples. These results could be important for bilayer and multilayer samples and offer a basis for spintronic and spin-orbitronic devices.

ACKNOWLEDGMENTS

This paper was supported by the program of the Institute of Problems of Chemical Physics, Russian Academy of Sciences (No. AAAA-A19-119092390079-8) and Grant of the President of the Russian Federation for Scientific School (No. 2644.2020.2). This paper was supported by the Institut Carnot ICEEL, by the impact project LUE-N4S, part of the French PIA project "Lorraine Université d'Excellence," Reference No. ANR-15-IDEX-04-LUE, and by the "FEDER-FSE Lorraine et Massif Vosges 2014–2020," the European Union, the Région Grand Est, the Metropole Grand Nancy, and the Chaire PLUS.

[1] F. Hellman, A. Hoffmann, Y. Tserkovnyak, G. S. D. Beach, E. E. Fullerton, C. Leighton, A. H. MacDonald, D. C. Ralph, D. A. Arena, H. A. Dürr, P. Fischer, J. Grollier, J. P. Heremans, T. Jungwirth, A. V. Kimel, B. Koopmans, I. N. Krivorotov, S. J. May, A. K. Petford-Long, J. M. Rondinelli *et al.*, Rev. Mod. Phys. **89**, 025006 (2017).

[2] R. Cardias, A. Szilva, M. M. Bezerra-Neto, M. S. Ribeiro, A. Bergman, Y. O. Kvashnin, J. Fransson, A. B. Klautau, O. Eriksson, and L. Nordström, Sci. Rep. **10**, 20339 (2020).

[3] M. Kuepferling, A. Casiraghi, G. Soares, G. Durin, F. Garcia-Sanchez, L. Chen, C. H. Back, C. H. Marrows, S. Tacchi, and G. Carlotti, arXiv:2009.11830v1.

[4] A. K. Zvezdin and A. P. Pyatakov, Europhys. Lett. **99**, 57003 (2012).

[5] K. Inoue, K. Kikuchi, M. Ohba, and H. Okawa, Angew. Chem. **42**, 4810 (2003).

[6] N. M. Vargas, F. Torres, A. A. Baker, J. R. I. Lee, M. Kiwi, T. M. Willey, C. Monton, and I. K. Schuller, Appl. Phys. Lett. **117**, 213105 (2020).

[7] P. M. Levy and A. Fert, Phys. Rev. B **23**, 4667 (1981).

[8] A. Fert and F. Nguyen Van Dau, C. R. Physique **20**, 817 (2019).

[9] V. Baltz, A. Manchon, M. Tsoi, T. Moriyama, T. Ono, and Y. Tserkovnyak, Rev. Mod. Phys. **90**, 015005 (2018).

[10] A. Hrabec, N. A. Porter, A. Wells, M. J. Benitez, G. Burnell, S. McVitie, D. McGrouther, T. A. Moore, and C. H. Marrows, Phys. Rev. B **90**, 020402(R) (2014).

[11] K. Shahbazi, J.-V. Kim, H. T. Nembach, J. M. Shaw, A. Bischof, M. D. Rossell, V. Jeudy, T. A. Moore, and C. H. Marrows, Phys. Rev. B **99**, 094409 (2019).

[12] F. Ajejas, V. Krizakova, D. de Souza Chaves, J. Vogel, P. Perna, R. Guerrero, A. Gudin, J. Camarero, and S. Pizzini, Appl. Phys. Lett. **111**, 202402 (2017).

[13] S.-G. Je, D.-H. Kim, S.-C. Yoo, B.-C. Min, K.-J. Lee, and S.-B. Choe, Phys. Rev. B **88**, 214401 (2013).

[14] R. Lavrijsen, D. M. F. Hartmann, A. van den Brink, Y. Yin, B. Barcones, R. A. Duine, M. A. Verheijen, H. J. M. Swagten, and B. Koopmans, Phys. Rev. B **91**, 104414 (2015).

[15] C. Moreau-Luchaire, C. Moutafis, N. Reyren, J. Sampaio, C. A. F. Vaz, N. Van Horne, K. Bouzehouane, K. Garcia, C. Deranlot, P. Warnicke, P. Wohlhuter, J.-V. George, M. Weigand, J. Raabe, V. Cros, and A. Fert, Nat. Nanotechnol. **11**, 444 (2016).

[16] P. Agrawal, F. Büttner, I. Lemesh, S. Schlotter, and G. S. D. Beach, Phys. Rev. B **100**, 104430 (2019).

[17] M. Bacani, M. A. Marioni, J. Schwenk, and H. J. Hug, Sci. Rep. **9**, 3114 (2019).

[18] S. P. Kang, H. Y. Kwon, H. S. Kim, J. H. Shim, and C. Won, J. Appl. Phys. **118**, 043905 (2015).

[19] L.-M. Li, B.-Z. Li, and F.-C. Pu, J. Phys.: Condens. Matter **6**, 1941 (1994).

[20] See Supplemental Material at http://link.aps.org/supplemental/10.1103/PhysRevB.104.134424 for hysteresis loops, X-ray spectrum, series of time dependences coordinate of the DDW, dependences of the velocities of the top and bottom DDW on the in-plane field and series of magnetic relaxation curves.

[21] R. B. Morgunov, A. V. Yurov, V. A. Yurov, A. D. Talantsev, A. I. Bezverhnii, and O. V. Koplak, Phys. Rev. B **100**, 144407 (2019).

[22] T. Fache, H. S. Tarazona, J. Liu, G. L'vova, M. J. Applegate, J. C. Rojas-Sanchez, S. Petit-Watelot, C. V. Landauro, J. Quispe-Marcatoma, R. Morgunov, C. H. W. Barnes, and S. Mangin, Phys. Rev. B **98**, 064410 (2018).

[23] A. Hamadeh, P. Pirro, J.-P. Adam, Y. Lu, M. Hehn, S. Petit Watelot, and S. Mangin, Appl. Phys. Lett. **111**, 022407 (2017).

[24] M. Heide, G. Bihlmayer, and S. Blügel, Phys. Rev. B **78**, 140403(R) (2008).

[25] N. Nakajima, T. Koide, T. Shidara, H. Miyauchi, H. Fukutani, A. Fujimori, K. Iio, T. Katayama, M. Nývlt, and Y. Suzuki, Phys. Rev. Lett. **81**, 5229 (1998).

[26] G. Delaney, D. Weaire, S. Hutzler, and S. Murphy, Philos. Mag. Lett. **85**, 89 (2005).

[27] Ng. K. Duong, R. Tomasello, M. Raju, A. P. Petrovic, S. Chiappini, G. Finocchio, and Ch. Panagopoulos, APL Mater. **8**, 111112 (2020).